LSDA+U study of cupric oxide: Electronic structure and native point defects

Dangxin Wu and Qiming Zhang
Department of Physics, University of Texas at Arlington, Arlington, Texas 76019, USA

Meng Tao
Department of Electrical Engineering, University of Texas at Arlington, Arlington, Texas 76019, USA
(Received 30 December 2005; revised manuscript received 20 April 2006; published 15 June 2006)

A first-principles study on strongly correlated monoclinic cupric oxide CuO has been performed by using the LSDA+U method. The optimized structural parameters of the crystal CuO are in good agreement with the experimental data. The electronic structures and magnetic properties calculated from the LSDA+U method show that, in its ground state, CuO is a semiconducting, antiferromagnetic material with an indirect band gap of 1.0 eV and local magnetic moment per unit formula of $0.60\mu_B$, which agree with the experimental results. The carrier effective masses in CuO are larger than those in silicon, indicating smaller carrier mobilities. We have also investigated native point defects in CuO. Our results show that CuO is intrinsically a *p*-type semiconductor because Cu vacancies are the most stable defects in both Cu-rich and O-rich environments.

DOI: 10.1103/PhysRevB.73.235206 PACS number(s): 71.20.Nr, 61.72.Ji

Due to its fundamental importance in understanding materials properties such as high-temperature superconductivity and its practical applications such as magnetic storage media,[1] gas sensors,[2] varistors,[3] catalysts,[4] and solar cells,[5] cupric oxide CuO has attracted increasing interest in the past decade. On the experimental side, x-ray diffraction[6] shows that the crystal structure of CuO is monoclinic with $C2/c$ symmetry and with four formula units per unit cell, as shown in Fig. 1. It is a *p*-type semiconductor with a reported band gap of 1.2–1.9 eV.[5,7–9] Neutron-scattering experiments reveal that CuO is antiferromagnetic below 220 K with a local magnetic moment per unit formula of $\sim 0.65\mu_B$.[10,12–14] Theoretically, the electronic structure of CuO has been studied using cluster model calculations[15] and other *ab initio* calculations based on the local spin-density approximation (LSDA).[16–18] These calculations failed to predict the semiconducting ground state, instead obtaining a nonmagnetic and metallic one for CuO. This is because CuO is a strongly correlated system[15] in which the strong electron-electron interactions should be considered in the calculations. One of the successful schemes to overcome this failure is the LSDA+U method[19–23] first proposed by Anisimov *et al.* They applied this method to CuO and obtained a correct electronic density of states.[19,22] However, the detailed band structure of CuO have not yet been obtained by this method. Also, there have been no theoretical investigations on native point defects in CuO so far. The formation of native point defects is important to a semiconductor. To make a *p-n* junction, both *p*-type and *n*-type doping are necessary. The existence of native defects may limit dopability in the material.

In this work, we present an LSDA+U calculation to thoroughly investigate the structural, electronic, and magnetic properties of CuO, including the band structure and the carrier effective masses. Native point defects in CuO are studied through the calculations of the formation energies, in which both the effects of chemical environment and Fermi level position are taken into account.

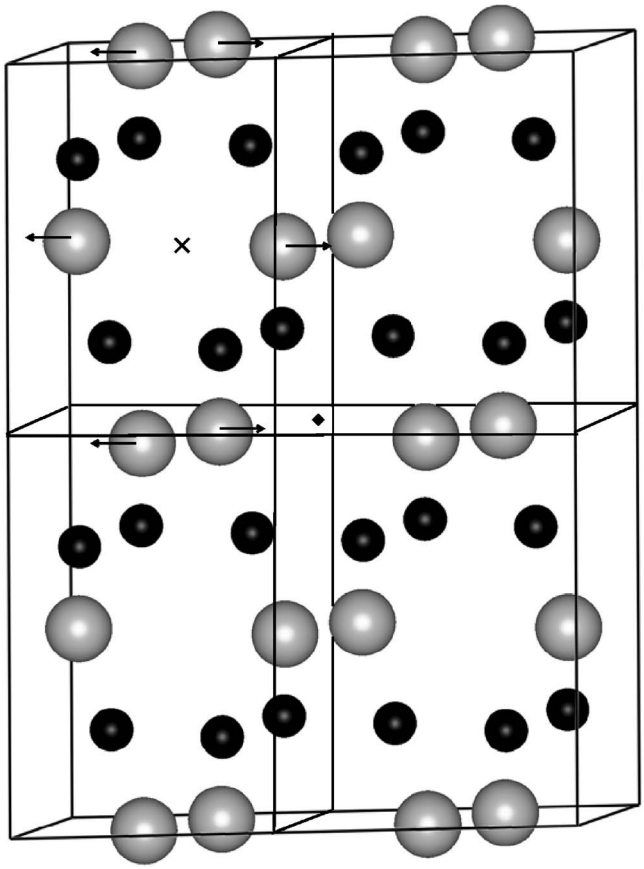

FIG. 1. The monoclinic unit cell of CuO. Dark balls indicate O atoms, while light balls indicate Cu atoms. The plot has been expanded as $2\times2\times1$ unit cells to give a better view. In the upper left unit cell, the local magnetic moment alignments of Cu atoms in the calculated antiferromagnetic ground state are indicated. The "×" indicates the most stable interstitial site. The "◆" indicates another possible high-symmetric interstitial site.

TABLE I. Lattice constants of monoclinic CuO. Two experimental measurements are listed for comparison. The notations of the structure follow Ref. 36.

Parameter	Experimental[a]	Experimental[b]	Theoretical (this work)
A (Å)	4.684	4.653	4.55
B (Å)	3.423	3.410	3.34
C (Å)	5.129	5.108	4.99
u	−0.582	−0.584	−0.582
β	99.54°	99.483°	99.507°

[a]Reference 6.
[b]Reference 36.

All the calculations in this work were performed using the VASP package.[25,27–30] In order to reduce the number of plane-wave basis functions necessary for accurately describing the electronic wave functions, the projector augmented wave (PAW) method[24–26] implemented in VASP was used in this work to describe the electron-ion interactions. The PAW potential for Cu was generated from the atomic configuration of $[\mathrm{Ar}]3d^{10}4s^1$. The $3d$ and $4s$ electrons were treated as valence electrons. For O, the atomic configuration to generate the PAW potential was $[\mathrm{He}]2s^2 2p^4$ and the $2s$ and $2p$ electrons were considered as valence electrons. At the level of the LSDA, the exchange-correlation functional proposed by Perdew and Zunger[31] based on the quantum Monte Carlo calculations of Ceperley and Alder[32] was used. For the LSDA+U method, we adopted the simplified rotationally invariant approach formulated by Dudarev *et al.*[33] The values of U and J for CuO, 7.5 and 0.98 eV, respectively, were adopted from Ref. 19, where the values were obtained from a constrained LDA calculation.[34]

To check the applicability and accuracy of both the LSDA+U method and the PAW method, we first performed calculations to optimize the structural parameters of crystal CuO. In these calculations, the integrations over the first Brillouin zone were made by using an $8\times8\times8$ k-point set generated according to the Γ centered Monkhorst-Pack scheme.[35] The plane-wave energy cutoff was set at 500 eV (36.75 Ry) to ensure the convergence of the calculations. Due to its low-symmetry monoclinic structure, the unit cell shape, lattice vectors, and atomic coordinates were optimized simultaneously at a series of fixed volumes and the total energies were calculated for each given volume. The optimized structural parameters corresponding to the smallest total energy are listed in Table I. Our calculated values are in good agreement with experiments, which justifies the LSDA+U method and the PAW potentials used in our following calculations.

Using the optimized structural parameters, calculations with the same k-point sampling set and energy cutoff were performed to study the ground-state magnetic properties and electronic structures. To find the magnetic properties, all possible magnetic moments corresponding to the ferromagnetic, antiferromagnetic, and nonmagnetic (paramagnetic) phases were initially assigned to the four Cu atoms in the unit cell. For example, 0 or $1\mu_B$ initial magnetic moment per Cu atom was assigned to the paramagnetic or ferromagnetic initial states, respectively. Self-consistent convergence was reached for each initial setting. There were several possible antiferromagnetic configurations for the four Cu atoms in the unit cell. By comparing the total energies obtained, as shown in Table II, we found that the lowest energy, i.e., the ground state of the crystal, corresponds to the antiferromagnetic phase indicated in Fig. 1. This is qualitatively in agreement with experiments, where CuO is found to be antiferromagnetic below 220 K.[10–14] The local magnetic moment per formula unit from our calculation is $0.60\mu_B$, which is also very close to experimental values obtained by neutron-scattering studies ($0.5-0.68\mu_B$).[10–12] The electronic structures, including band structures and density of states (DOS), of CuO were calculated by using the LSDA+U method. To find out the effects of the Hubbard U on this system, we also used the LSDA method to obtain the electronic structures using the same optimized structural parameters and energy cutoffs. The DOS of CuO from the calculations based on both the LSDA and LSDA+U methods are compared in Fig. 2. First, the symmetric DOS for both spin up and spin down indicates an antiferromagnetic ground state, consistent with the local magnetic moment results as shown in Fig. 1. While the DOS calculated from the LSDA method exhibits a metallic character in that the spin-polarized DOS is nonzero at the Fermi level, the LSDA+U approach leads to a different picture of the DOS of CuO, with zero DOS at the Fermi level and an indirect energy gap of 1.0 eV. Therefore, by introducing the Hubbard U, the LSDA+U method predicts CuO to be a semiconductor, which agrees well with experiments, correcting the results from the LSDA method. The above results can be seen more clearly in the band structures of CuO. The band structures of CuO along high-symmetry directions of the first Brillouin zone calculated by the LSDA and LSDA+U methods are shown in Figs. 3 and 4. Our calculated band structure

TABLE II. The energy differences for the various magnetic phases in the CuO unit cell. The zero point of the energy is chosen as the ground-state antiferromagnetic configuration whose magnetic moments are indicated by the arrows in Fig. 1.

Magnetic configuration	Initial magnetic moment (μ_B) for each of the four Cu atoms	Energy difference per Cu atom (meV)
Antiferromagnetic (ground state)	+1, −1, +1, −1	0
Other antiferromagnetic states	+1, +1, −1, −1	7–63
Paramagnetic	0, 0, 0, 0	265
Ferromagnetic	+1, +1, +1, +1	55

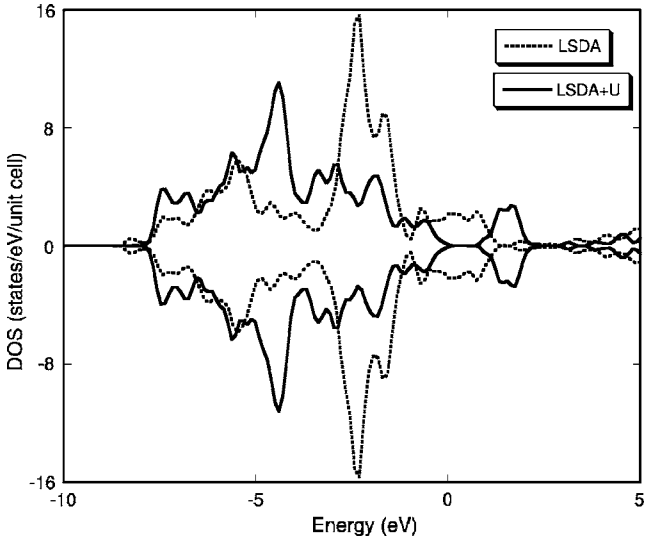

FIG. 2. Comparison of density of states of CuO from LSDA (dotted lines) and LSDA+U (solid lines) calculations. The positive and negative DOS refers to spin up and spin down, respectively. The energy zero point is chosen at Fermi level.

using the LSDA method (Fig. 3), consistent with that calculated previously by the LSDA-based orthogonalized linear combination of atomic orbitals method,[18] shows clearly that two conduction bands have dropped and cross the Fermi

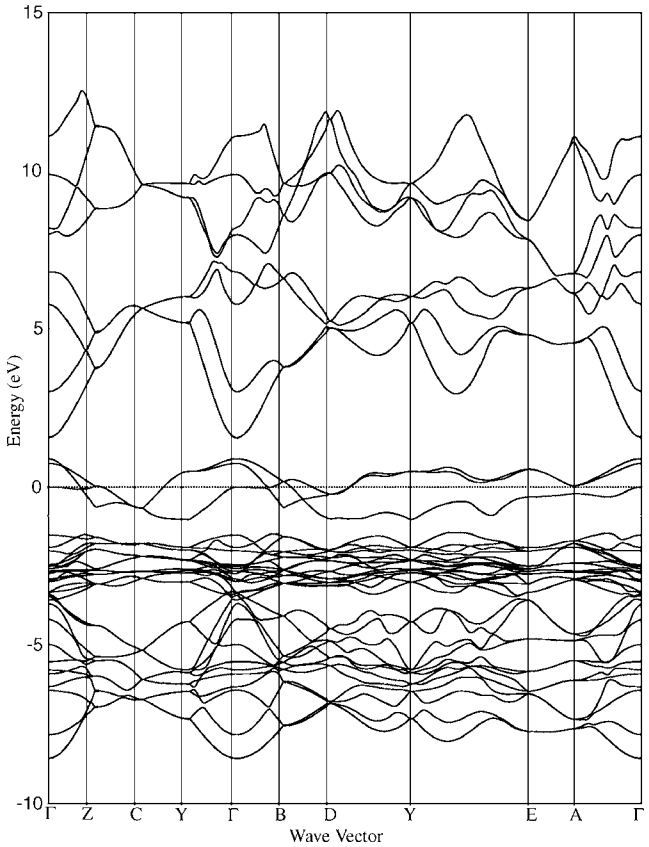

FIG. 3. Band structure of CuO from LSDA calculations. The Fermi level (dashed line) is set at 0 eV. The notations of the high-symmetry points of the first Brillouin zone follow Ref. 37.

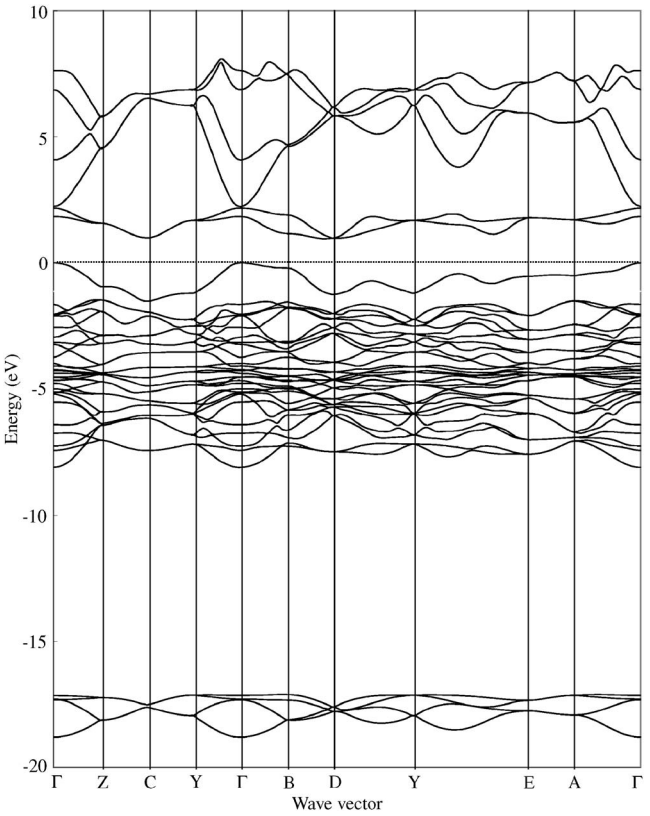

FIG. 4. Band structure of CuO from LSDA+U calculations. The Fermi level (dashed line) is set at 0 eV. The notations of the high-symmetry points of the first Brillouin zone follow Ref. 37.

level, which is set at 0 eV. Therefore no energy gap appears, predicting a metallic or semimetallic ground state for CuO. On the other hand, the band structure by the LSDA+U method (Fig. 4) shows no conduction band crossing by the Fermi level. The two conduction bands crossed by the Fermi level in the LSDA calculations are pushed upward from the Fermi level by the introduction of the Hubbard U. As a consequence, an indirect energy gap of 1.0 eV appears and CuO is predicted to be a semiconductor in its ground state, which is confirmed by several experiments.[5,8,9] From the analysis of the wave functions, the top valance band and the two bottom conduction bands are attributed to the $3d$ orbitals of Cu atoms. The LSDA+U method improved the treatment to the localized $3d$ states from Cu, leading to the correct electronic structure of CuO.

To have a picture about the carrier mobility in CuO, we also calculated the effective masses in CuO using the LSDA+U method. The minimum of the conduction band is at point $D(\frac{1}{2},0,\frac{1}{2})$ in Fig. 4. The longitudinal direction is along $D\Gamma$, while the transverse effective masses were calculated in the plane perpendicular to it. The calculated longitudinal and transverse electron effective masses are $0.78m_0$ and $3.52m_0$, respectively, where m_0 is the rest mass of a free electron. The average hole effective mass is $1.87m_0$. Compared with silicon, whose effective masses are $0.26m_0$ and $0.39m_0$ for electrons[38] and holes,[39] respectively, the carrier mobilities in CuO are much smaller. As stated earlier, since both the top of valance band and the bottom of conduction

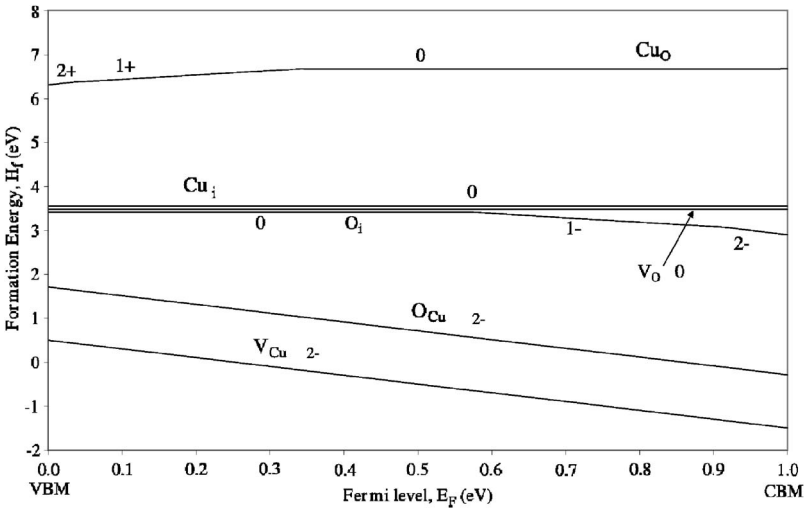

FIG. 5. Formation energies of native point defects in CuO as a function of the Fermi level E_F, varying from the valence-band maximum (VBM) to the conduction-band minimum (CBM) in the O-rich environment. The native defects include Cu vacancy (V_{Cu}), Cu interstitial (Cu_i), O vacancy (V_O), O interstitial (O_i), and two antisite defects (Cu_O or O_{Cu} where A_B means "*B*" atom is replaced by "*A*" atom). The charge state is indicated by the number with a sign [the "*q*" in Eq. (1)] next to the corresponding line. For each defect species, only the lowest-energy charge state at a given E_F is shown.

band of CuO are Cu 3*d* orbital dominated, the curvature are smaller than those in Si where the states are *s*-*p* hybrid. The 3*d* electrons are also more localized compared with *sp* electrons. This may explain why the carrier mobilities in CuO are much smaller than those in Si.

After a clearer picture of the crystalline CuO, we then focused on native point defects in CuO. In this study, a larger supercell is necessary to avoid the artificial interaction of neighboring defects due to the periodic boundary conditions. To calculate the formation energies of native point defects in CuO, we constructed a supercell as large as $2\times3\times2$ unit cells based on the optimized structural parameters. This supercell contains 96 atoms in a perfect crystal structure. We considered three different types of native point defects: vacancies (V_{Cu} or V_O, where the subscript refers to the missing host atom), antisite defects (Cu_O or O_{Cu} where A_B means "*B*" atom is replaced by "*A*" atom) and isolated interstitials (O_i or Cu_i). A vacancy was introduced by removing a Cu atom or O atom from the supercell. For the antisite defects, an O atom was replaced by a Cu atom or a Cu atom was substituted by an O atom in the supercell. In the case of isolated interstitials, an atom of Cu or O was put in possible high-symmetry interstitial sites in the supercell, as shown in Fig. 1 by "×" and "◆." The central "empty" position of the unit cell (as indicated as "×" in Fig. 1) was considered as a possible interstitial site. After a defect was introduced, all the atoms were allowed to relax according to the Hellmann-Feynman forces. For these calculations, the *k*-point sampling in the first Brillouin zone was carried out only at the Γ point due to the large size of the supercell, which greatly increased the computational efforts. This was justified by comparing the differences in formation energies of a few randomly selected defects between the calculation with only the Γ-point sampling and the one with a $2\times2\times2$ *k*-point sampling. The differences are less than 0.1 eV, which is much less than the formation energy differences between the different defects in the following discussion.

Based on the standard formalism proposed by Zhang and Northrup,[40] the formation energy H_f for an intrinsic defect with charge *q* (including its sign, *q* is the number of electrons transferred from the defect to the reservoirs) in CuO can be expressed as a function of electron Fermi level as well as atomic chemical potentials:

$$H_f = E_T(\text{defect};q) - E_T(\text{perfect}) - n_{Cu}\mu_{Cu} - n_O\mu_O + qE_{VBM} + qE_F, \quad (1)$$

where $E_T(\text{defect};q)$ and $E_T(\text{perfect})$ are the total energies of a supercell with and without the defect, respectively, $n_{Cu}(n_O)$ denotes the number of Cu (O) atoms removed from or added into the perfect supercell (e.g., $n_{Cu}=-1$ and $n_O=0$ for Cu vacancy; $n_{Cu}=+1$ and $n_O=0$ for Cu interstitial) and μ_{Cu} (μ_O) is the corresponding chemical potential. E_{VBM} is the energy of the valence-band maximum (VBM) of the perfect system and E_F is the electron Fermi energy referenced to the VBM of the host ($E_F=0$ when the Fermi level is at VBM), which could be thought as the chemical potential for electrons. By adding the term qE_{VBM}, the zero point of the single electron energy level is shifted to a well-defined position, i.e., VBM. The chemical potentials depend on the experimental growth conditions, which can be Cu rich or O rich, and anything in between. Under Cu-rich conditions, Cu is assumed to be in a thermodynamic equilibrium with the bulk Cu and therefore $\mu_{Cu}=\mu_{Cu[bulk]}$, where $\mu_{Cu[bulk]}$ is the total energy per atom of metallic Cu. The O chemical potential in this case is not independent but constrained by the equilibrium condition

$$\mu_O + \mu_{Cu} = \mu_{CuO}. \quad (2)$$

Under O-rich conditions, O is assumed to be in equilibrium with O_2 gas, so its chemical potential is $\mu_{O[gas]}$, the total energy per atom of molecular O_2. In this case, μ_{Cu} is determined by Eq. (2). To obtain $\mu_{Cu[bulk]}$ and $\mu_{O[gas]}$, separate calculations are performed to get the total energies of metallic Cu with fcc structure and molecular O_2. For metallic Cu, a $16\times16\times16$ *k*-point set is generated by the Monkhorst-Pack scheme. The optimized lattice parameter is 3.52 Å, which is in good agreement with the experimental value of 3.61 Å.[36] In the case of O_2, a very large (25-Å cubic) supercell and Γ-point sampling are used. The optimized O-O bond length for the triplet ground state is 1.22 Å, very close to the experimental value of 1.21 Å.[41]

Figure 5 shows the formation energies H_f for various native point defects in CuO as a function of the Fermi level E_F in the O-rich environment. In the Cu-rich environment, the plot (not shown) is very similar to Fig. 5 because of the close

values of the calculated chemical potentials of Cu in both cases. For each defect species, all the atoms in the supercell were relaxed according to the Hellmann-Feymann forces on them. The optimization continued until the forces were all smaller than 10^{-3} atomic unit. For charged state, an opposite but uniformly distributed charge was introduced to keep the supercell electrically neutral. The calculated total energy was used as the first term in Eq. (1). Since the formation energies vary linearly with E_F, several straight lines with different slopes would be generated for each defect species but different charge states. In Fig. 5, only the lowest-energy charge state at the given E_F is shown. From the graph, we can see that while the stable charge state of some defect species varies with the position of the Fermi level, other defects have only one stable charge state in the whole range of the Fermi level. For example, V_{Cu}^{2-}, where the superscript refers to the charge $q(-2)$ of the defect, is always the most stable defect in Cu vacancies. It can be seen that in *p*-type CuO when the Fermi level is close to E_{VBM} (E_F=0 eV), the stable charge state for each defect is Cu_O^{2+}, Cu_i^0, V_O^0, O_i^0, O_{Cu}^{2-} and V_{Cu}^{2-}. On the other hand, in *n*-type CuO when the Fermi level is close to the conduction-band minimum (CBM) (E_F =1.0 eV), Cu_O^0, Cu_i^0, V_O^0, O_i^{2-}, O_{Cu}^{2-}, and V_{Cu}^{2-} are the most stable defects. An important conclusion we can draw from the graph is that V_{Cu}^{2-} always has the lowest formation energy (less than 1.0 eV), indicating that there is a spontaneous Cu vacancy formation during the growth of crystal CuO. Since the negative charged state, V_{Cu}^{2-} is always the lowest among the other charged states of the defect, an undoped CuO should be dominated by acceptors. This means that intrinsically, CuO is a *p*-type semiconductor. This result is in agreement with many experiments.[5,7–9]

In summary, we have performed a first-principles calculation using the LSDA+U method to investigate the structural, electronic, and magnetic properties of crystal CuO, as well as the formation energies of native point defects in it. The optimized structural parameters from our calculations agree well with experimental values. The band structure and density of states of CuO are then calculated. The calculations show that CuO is a semiconductor with an indirect band gap of 1.0 eV, which agrees well with experimental results. It is a significant improvement over the LSDA calculation which obtains a metallic ground state for CuO. Our calculations also point to an antiferromagnetic CuO, which is consistent with neutron scattering experiments. By studying the formation energies of native point defects in CuO, we conclude that Cu vacancies are the most stable defects in CuO in both Cu-rich and O-rich environments, which indicates that CuO is intrinsically a *p*-type semiconductor. This result agrees with several experiments.

We are grateful to Longcheng Wang for beneficial discussions. This work was supported in part by the National Science Foundation (Grant No. ECS-0322762-2003) and the Petroleum Research Fund (Grant No. 38563-AC5).

[1] R. V. Kumar, Y. Diamant, and A. Gedanken, Chem. Mater. **12**, 2301 (2000).
[2] P. Poizot, S. Laruelle, S. Grugeon, and J. M. Taracon, Nature (London) **407**, 496 (2000).
[3] Y. Jiang, S. Decker, C. Mohs, and K. J. Klabunde, J. Catal. **180**, 24 (1998).
[4] T. Ishihara, M. Higuchi, T. Takagi, M. Ito, H. Nishiguchi, and T. Takita, J. Mater. Chem. **8**, 2037 (1998).
[5] S. C. Ray, Sol. Energy Mater. Sol. Cells **68**, 307 (2001).
[6] S. Åsbrink and L.-J. Norrby, Acta Crystallogr., Sect. B: Struct. Crystallogr. Cryst. Chem. **26**, 8 (1970).
[7] K. L. Hardee and A. J. Bard, J. Electrochem. Soc. **124**, 215 (1977).
[8] F. P. Koffyberg and F. A. Benko, J. Appl. Phys. **53**, 1173 (1982).
[9] F. Marabelli, G. B. Parravicini, and F. Salghetti-Drioli, Phys. Rev. B **52**, 1433 (1995).
[10] J. B. Forsyth, P. J. Brown, and B. M. Wanklyn, J. Phys. C **21**, 2917 (1988).
[11] B. X. Yang, J. M. Tranquada, and G. Shirane, Phys. Rev. B **38**, 174 (1988).
[12] B. X. Yang, T. R. Thurston, J. M. Tranquada, and G. Shirane, Phys. Rev. B **39**, 4343 (1989).
[13] P. J. Brown, T. Chattopadhyay, J. B. Forsyth, V. Nunez, and F. Tasset, J. Phys.: Condens. Matter **3**, 4281 (1991).
[14] M. Aïn, A. Menelle, B. M. Wanklyn, and E. F. Bertaut, J. Phys.: Condens. Matter **4**, 5327 (1992).
[15] J. Ghijsen, L. H. Tjeng, J. van Elp, H. Eskes, J. Westerink, G. A. Sawatzky, and M. T. Czyzyk, Phys. Rev. B **38**, 11322 (1988).
[16] K. Terakura, T. Oguchi, A. R. Williams, and J. Kubler, Phys. Rev. B **30**, 4734 (1984).
[17] M. Grioni, M. T. Czyzyk, F. M. F de Groot, J. C. Fuggle, and B. E. Watts, Phys. Rev. B **39**, 4886 (1989).
[18] W. Y. Ching, Y.-N. Xu, and K. W. Wong, Phys. Rev. B **40**, 7684 (1989).
[19] V. I. Anisimov, J. Zaanen, and O. K. Andersen, Phys. Rev. B **44**, 943 (1991).
[20] M. T. Czyzyk and G. A. Sawatzky, Phys. Rev. B **49**, 14211 (1994).
[21] A. I. Liechtenstein, V. I. Anisimov, and J. Zaanen, Phys. Rev. B **52**, R5467 (1995).
[22] V. I. Anisimov, F. Aryasetiawan, and A. I. Liechtenstein, J. Phys.: Condens. Matter **9**, 767 (1997).
[23] W. E. Pickett, S. C. Erwin, and E. C. Ethridge, Phys. Rev. B **58**, 1201 (1998).
[24] P. E. Blöchl, Phys. Rev. B **50**, 17953 (1994).
[25] G. Kresse and D. Joubert, Phys. Rev. B **59**, 1758 (1999).
[26] O. Bengone, M. Alouani, P. Blöchl, and J. Hugel, Phys. Rev. B **62**, 16392 (2000).
[27] G. Kresse and J. Hafner, Phys. Rev. B **47**, R558 (1993).
[28] G. Kresse and J. Hafner, Phys. Rev. B **49**, 14251 (1994).
[29] G. Kresse and J. Furthmüller, Phys. Rev. B **54**, 11169 (1996).
[30] G. Kresse and J. Furthmüller, Comput. Mater. Sci. **6**, 15 (1996).
[31] J. P. Perdew and A. Zunger, Phys. Rev. B **23**, 5048 (1981).
[32] D. M. Ceperley and B. J. Alder, Phys. Rev. Lett. **45**, 566 (1980).

[33] S. L. Dudarev, G. A. Botton, S. Y. Savrasov, C. J. Humphreys, and A. P. Sutton, Phys. Rev. B **57**, 1505 (1998).
[34] O. Gunnarsson, O. K. Andersen, O. Jepsen, and J. Zaanen, Phys. Rev. B **39**, 1708 (1989).
[35] H. J. Monkhorst and J. D. Pack, Phys. Rev. B **13**, 5188 (1976).
[36] R. W. G. Wyckoff, *Crystal Structures* (Interscience Publishers, New York, 1963).
[37] M. Lax, *Symmetry Principles in Solid State and Molecular Physics* (Dover Publications, New York, 2001).
[38] R. N. Dexter, B. Lax, A. F. Kip, and G. Dresselhaus, Phys. Rev. **96**, 222 (1954).
[39] R. N. Dexter and B. Lax, Phys. Rev. **96**, 223 (1954).
[40] S. B. Zhang and J. E. Northrup, Phys. Rev. Lett. **67**, 2339 (1991).
[41] D. R. Lide, *CRC Handbook of Chemistry and Physics* (CRC Press, New York, 1998).